15

Hydrogen and Methane Storage in MOFs

15.1 Introduction

Hydrogen is considered an ideal clean energy source because water is the sole product of its combustion and no greenhouse gases or other environmentally harmful compounds are released. Natural gas (NG) is considered an environmentally friendly fossil fuel because its main component, methane (CH_4), has the highest research octane number (RON = 107) among all hydrocarbons and consequently its combustion releases the smallest amount of CO_2. Both hydrogen and natural gas provide the prospect to supersede fossil fuels and thus provide cleaner energy sources.

To commercialize energy systems driven by H_2 or NG, storage materials must be developed. Porous materials have been intensely studied during the past decades owing to their ability to adsorb gases at comparatively low pressures. With respect to energy storage, metal-organic frameworks (MOFs) have attracted a growing interest owing to their modular and highly tunable nature. Their structures combine high surface areas, low densities, and facile functionalization. This allows for the development of storage materials with high gravimetric and volumetric uptake – an outstanding challenge that must be addressed to make gaseous fuels viable alternatives to liquid fossil fuels. For the down-selection of materials for this type of application, characteristics such as the working capacity, system capacity, and cycling stability gain in importance. These terms have been defined in Chapter 13.

For hydrogen and natural gas storage in MOFs, upper pressure limits of 35 or 65 bar (maximum pressure achievable with inexpensive single-stage and dual-stage compressors, respectively) and a lower pressure limit of 5 bar (minimum inlet pressure) are typically reported [1]. This implies that in order to maximize the working capacity, not only the storage capacity at high pressures (35–65 bar) needs to be maximized but the amount of gas retained at pressures below 5 bar should also be minimized (see Figure 13.2). In mobile applications such as the installation of adsorbent-based tanks in automobiles, the cycle life requirements are that the storage material should surpass the expected life of the vehicle (more than 250 000 km or 155 343 miles), which equals about 1500 charge–discharge cycles. This prerequisite implies that onboard gas storage

Introduction to Reticular Chemistry: Metal-Organic Frameworks and Covalent Organic Frameworks,
First Edition. Omar M. Yaghi, Markus J. Kalmutzki, and Christian S. Diercks.

Companion website: www.wiley.com/go/yaghi/reticular

systems require materials possessing chemical and architectural stability with respect to cycling, temperature swings of up to 125 °C, and mechanical stress such as vibrations and rattling.

15.2 Hydrogen Storage in MOFs

Hydrogen is an ideal replacement for petroleum especially in automotive applications because it is a zero-emission fuel, abundantly available, and, when liquefied, has approximately triple the energy density of gasoline. While hydrogen is the third most abundant element on the Earth's surface, hydrogen gas (H_2) is very rare (less than 1 ppm per volume) [2]. Gaseous hydrogen is commonly produced by electrolysis of water or steam reforming of natural gas (Figure 15.1). Since the production of hydrogen requires other sources of energy it is considered an energy carrier rather than an energy source.

To use hydrogen in everyday applications the methods of hydrogen production, delivery, and storage, as well as the fuel cell technology must be further developed. Hydrogen storage is considered to play a key role in this development. Current methods of chemical and physical storage present several disadvantages. Metal hydrides, boranes, or imidazolium ionic liquids for chemical storage of hydrogen are often associated with high production costs alongside unfavorable kinetics and a high susceptibility toward contaminations that are typically present in hydrogen gas. Cryogenic storage of liquid hydrogen is accompanied by high operational costs and an increased weight of the cryogenic tanks, rendering it almost impractical. Physical storage of liquid hydrogen has been used by NASA (National Aeronautics and Space Administration) to propel space shuttles into orbit since the 1970s and today some vehicles including buses and trains run on pressurized hydrogen. The high volatility of hydrogen at ambient conditions aggravates the physical storage in pressurized tanks that commonly sustains only low volumetric energy densities, even when expensive multistage compressor systems are used to achieve pressures of up to 300 bar in heavy reinforced tanks. To make hydrogen a fuel that is more germane for everyday applications, low-cost lightweight materials capable of reversible hydrogen uptake (at ambient conditions) and storage densities equal to or even greater than that of liquid hydrogen are needed.

The US Department of Energy (DOE) 2020 targets for hydrogen storage systems are a gravimetric uptake of 0.055 $kg_{(H_2)}$ kg^{-1} and a volumetric capacity of 0.00445 $kg_{(H_2)}$ l^{-1}, while retaining short refueling times and high cycling stability at operating temperatures between 30 and 50 °C. It should be noted that these are requirements for an entire storage system; hence, the performance of the storage material itself must exceed them to compensate for system-based losses (see Chapter 13). Figure 15.2 illustrates how far these requirements can be met by MOF-5.

(a) $CH_4 + H_2O \rightleftharpoons CO + 3H_2$

(b) $2H_2O(l) \underset{\text{Combustion}}{\overset{\text{Electrolysis}}{\rightleftharpoons}} 2H_2 + O_2$

Figure 15.1 Reaction equation for the production of hydrogen gas by (a) steam reforming and (b) electrolysis of water.

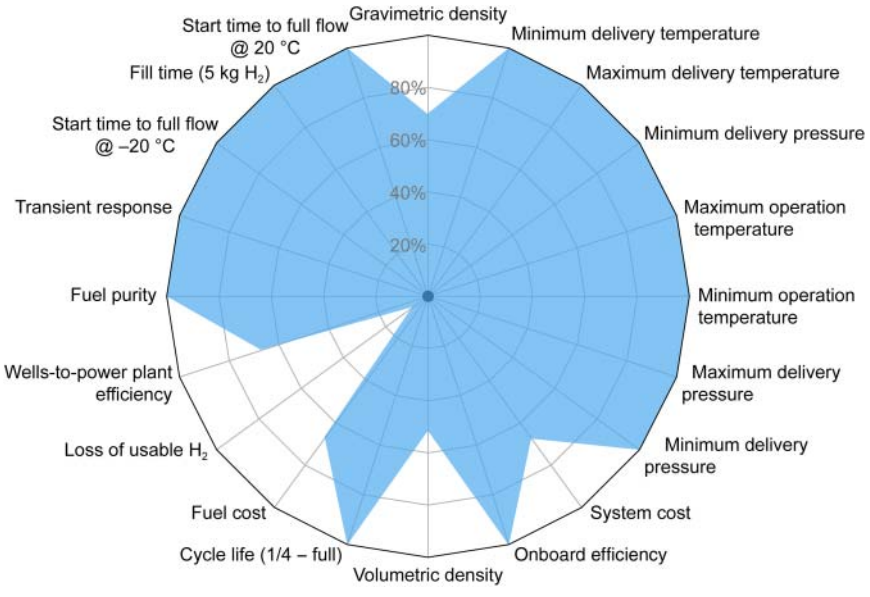

Figure 15.2 Spider graph showing a comparison of the hydrogen storage performance of MOF-5 to the 2020 DOE (Department of Energy) targets. Shown is the data for a projected system (100 bar, 80–160 K, Type I tank, hexcell-loose powder) (https://energy.gov/eere/fuelcells/hydrogen-storage-engineering-center-excellence). Many of the targets set by the DOE have already been achieved; however, further development is needed to render MOFs suitable candidates for large-scale applications.

15.2.1 Design of MOFs for Hydrogen Storage

To design a MOF suitable for hydrogen storage and to optimize it with respect to its storage properties, it is instructive to take a closer look at the interactions between hydrogen and the framework skeleton. Hydrogen can interact with the framework in two ways: physisorption through weak dispersive interactions with the backbone of the framework and strong interactions with specific adsorption sites. The former requires high surface areas to achieve a large hydrogen uptake while the latter requires the introduction of strong adsorption sites into the framework architecture (e.g. open metal sites). Both interactions can be realized in MOFs because they combine high surface areas, low densities, tunable pore sizes, and the possibility for the introduction of specific adsorption sites. General aspects of the design of such structures were discussed in Chapters 1–6. With respect to hydrogen storage, MOFs built from light metals such as Be^{2+}, Al^{3+}, or Mg^{2+} are of interest because they promise to show a high gravimetric uptake in addition to the high volumetric uptake, originating from their highly porous nature. It should be noted that in the temperature regime targeted by the DOE, dispersive forces alone do not lead to substantial hydrogen uptake. Consequently, a polar/polarizable pore environment is required to provide for strong interactions between the pore walls and hydrogen molecules. In the following, we will discuss structural factors that lead to high hydrogen storage capacities,

design principles for hydrogen storage materials, and approaches for the optimization of promising candidates.

15.2.1.1 Increasing the Accessible Surface Area

The amount of physisorbed gas in a porous solid is proportional to its surface area. Therefore, it seems reasonable to design materials with high surface areas when targeting a large maximum storage capacity. However, the pore size should be tailored to the specific kinetic diameter of the gas in question, and it is advantageous to design the pores in such a way as to maximize the interaction between their surface and the hydrogen molecules.

Expansion of the Linker Strategies to increase the surface area have been discussed in Chapter 2 where we have introduced an approach for the design of linkers that facilitate the preparation of MOFs with ultrahigh surface areas. We illustrated that trigonal linker molecules based on a 1,3,5-triphenylbenzene core unit are ideal building units for this purpose and showed a series of MOFs (MOF-177, MOF-180, and MOF-200) designed with this idea in mind. Here, the same MOFs (MOF-177 and MOF-200) will help us to determine the correlation between the surface area and the hydrogen storage capacity. MOF-177 and MOF-200 are both built from trigonal tritopic linkers and octahedral $Zn_4O(–COO)_6$ secondary building units (SBUs) and have a **qom** topology (see Figure 2.16) [3]. MOF-177 has a geometric surface area of 4740 $m^2\ g^{-1}$, and with 6400 $m^2\ g^{-1}$ the geometric surface area of the expanded analog MOF-200 is even larger. Consequently, MOF-200 shows a higher hydrogen uptake (163 $mg\ g^{-1}$) compared to MOF-177 (75 g mg g^{-1}) [3, 4]. In general, we can say that for isoreticular frameworks the one with the higher surface area also has the higher hydrogen uptake (at low pressures). Aside from the surface area, the structure type (topology) of the framework, along with the consequential pore shapes and metrics, has a big influence on the hydrogen storage capacity. Increasing the surface area by applying the mixed linker approach is therefore often more promising since this frequently leads to high surface areas and complex pore systems that consist of many connected small pores (see Chapter 6). This strategy is used in the design of MOF-205 (**ith-d**) and MOF-210 (**toz**), two tertiary MOFs built from trigonal tritopic linkers, linear ditopic linkers, and octahedral $Zn_4O(–COO)_6$ SBUs [3]. Even though MOF-205 has a lower geometric surface area (4680 $m^2\ g^{-1}$) than MOF-200 (6400 $m^2\ g^{-1}$), its hydrogen uptake (7 wt%) is close to that of MOF-200 (7.4 wt%). MOF-210 has a higher surface area (6240 $m^2\ g^{-1}$) than MOF-205 while maintaining comparatively small pores, which leads to a maximum hydrogen uptake of 8.6 wt%. These findings support the idea that a large surface area leads to a high hydrogen uptake, whereas increasing the pore size above a critical diameter does not help increase the hydrogen uptake. Figure 15.3 shows the correlation between the hydrogen storage capacity of several MOFs and their respective surface areas.

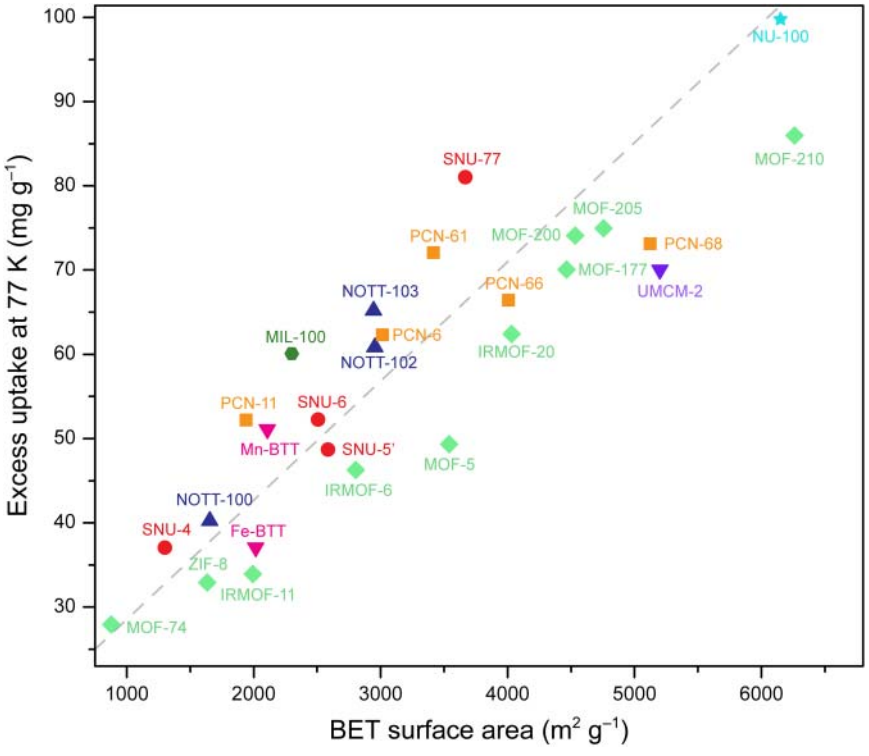

Figure 15.3 Plot of the BET surface area ($m^2\ g^{-1}$) of a compilation of highly porous MOFs versus the hydrogen excess uptake (mg g^{-1}) at 77 K. The gray dotted line represents the trend line that illustrates that the hydrogen adsorption capacity at 77 K correlates strongly with the surfae area.

Interpenetrated Frameworks Hydrogen uptake capacity is not governed by the surface area alone. Different MOFs with similar surface areas exhibit different values for their respective excess hydrogen uptake. This is explained by the difference in their structure or, more specifically, their pore metrics and the fact that some of them are interpenetrated. Interpenetration has a dramatic effect on the pore size but not necessarily on the pore volume. Consequently, interpenetrated structures frequently show a higher excess uptake than their non-interpenetrated counterparts that have similar surface areas but large pores. Smaller pores allow for a stronger interaction between the framework and hydrogen molecules. The optimal pore size for hydrogen adsorption at room temperature is predicted to be approximately 7 Å based on calculations on idealized homogeneous materials. Slit-shaped pores of 7 Å diameter allow for the adsorption of one layer of hydrogen molecules on opposing surfaces, thus minimizing the empty volume of the pore while maximizing the van der Waals interaction of hydrogen with the framework. At cryogenic temperatures

the formation of a H_2-sandwich in between two opposing pore surfaces is highly favorable, and the ideal pore size for maximum volumetric hydrogen uptake at 100 bar increases to 10 Å regardless of the pore shape.

15.2.1.2 Increasing the Isosteric Heat of Adsorption

The amount of gas that can be adsorbed on the surface of a framework material is proportional to its surface area. With respect to hydrogen this is only true at cryogenic temperatures and indeed, some MOFs with ultrahigh surface areas meet the DOE targets for hydrogen uptake in terms of weight percent (<5.5 wt%) at cryogenic temperatures. In contrast, a significant drop in the maximum hydrogen uptake is typically observed at elevated temperatures. This is ascribed to the weak van der Waals interactions involved in the physisorption of hydrogen molecules within the framework and results in less than 1/10 of the cryogenic uptake at ambient temperatures. For application in mobile adsorbent-based hydrogen storage tanks, however, storage capacities >5.5% at ambient temperatures are required. This in turn means that stronger adsorption sites are needed to meet this requirement. How strongly a molecule is bound to the surface is defined by the isosteric heat of adsorption (Q_{st}), which is correlated to the strongest interaction between the gas molecules and the framework. Therefore, the affinity of the framework toward hydrogen at ambient temperatures can be optimized by increasing Q_{st}, thus allowing for stronger interactions and thereby higher hydrogen uptake at elevated temperatures. This means that aside from a large free pore volume, the magnitude of Q_{st} is the most important factor in achieving high hydrogen adsorption capacities [5]. The optimum Q_{st} value for high-pressure applications is approximately 20 kJ mol^{-1}.The Q_{st} values for hydrogen adsorption in most MOFs is however in the range of 5–9 kJ mol^{-1} [6]. In this section we will outline way to increase the isosteric heat of adsorption through precise adjustment of structural parameters.

Open Metal Sites and Other Coordinatively Unsaturated Metal Centers The interaction between hydrogen molecules and coordinatively unsaturated metal centers has been studied in molecular chemistry for decades. Figure 15.4 shows the orbitals involved in a side-on coordination of hydrogen to a metal center. The σ-electrons of H_2 interact with the vacant metal d-orbitals of the metal and occupied d-orbitals of the metal donate electrons into the σ*-orbitals of H_2 by backdonation.

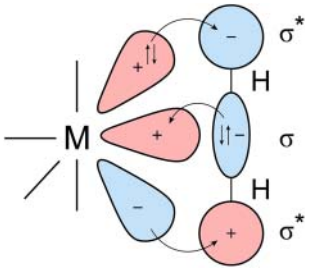

Figure 15.4 Side-on coordination of H_2 to a metal complex. The H_2-σ orbital can bind to a metal-centered σ orbital. Electron density is transferred to the σ* orbital of H_2 by backbonding.

Dissociation energies of 80–90 kJ mol^{-1} have been determined for complexes such as $(C_5H_5)V(CO)_3(H_2)$ and $Mo(CO)_5(H_2)$ [7]. These values are too high for the purpose of gas storage because it takes tremendous amounts of energy (i.e. heat) to liberate the adsorbed hydrogen gas. Desired binding energies for hydrogen storage are within the regime of charge-induced dipole interactions (~20 kJ mol^{-1}); hence, favorable orbital interactions leading to strong metal–H_2 bonds must be avoided. Binding energies in this regime have been observed for interactions between H_2 and Li^+ in the gas phase (~27 kJ mol^{-1}) and consequently the intercalation of Li^+ into porous frameworks (in particular, covalent organic frameworks [COFs]) has been studied. In such materials the charge of the lithium ions is however partially quenched and the heat of adsorption is therefore significantly reduced. Nonetheless, the intercalation of Li^+ into COFs results in a significantly enhanced hydrogen storage capacity. The storage capacity of COF-202 increases from 8.08 g l^{-1} and 1.52 wt% to 25.86 g l^{-1} and 4.39 wt% upon lithium doping, and COF-105 and COF-108 both surpass the DOE target of 6 wt% with 6.73 and 6.84 wt% at 100 bar and 298 K, respectively [8]. Similar effects are achieved by intercalation with other metal ions such as those of Ca, Sc, and Ti, and this approach is also applicable to MOFs [9].

Another way to incorporate coordinatively unsaturated metal centers is the formation of open metal sites in MOFs. Such Lewis acidic sites are considered the most promising way of increasing the isosteric heat of hydrogen adsorption and they are typically formed by removal of terminal ligands from specific SBUs by heating the MOF in dynamic vacuum. Figure 15.5 shows some SBUs with

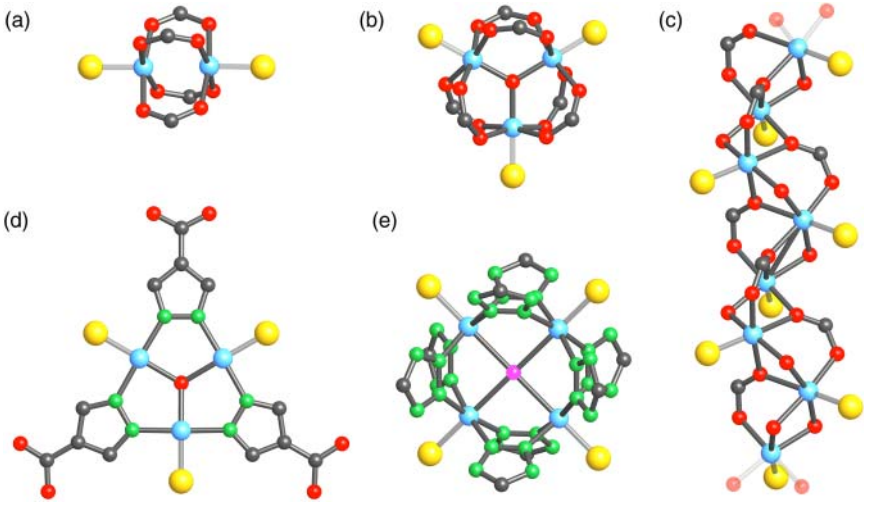

Figure 15.5 SBUs with potential open metal sites. The terminal ligands whose removal leads to the formation of open metal sites are represented by yellow spheres. (a) Square tetratopic $M_2L_2(–COO)_4$ paddle wheel SBU, (b) trigonal prismatic hexatopic $M_3OL_3(–COO)_6$ SBU, (c) rod-like $[M_3O_2L_2(COO)_3]_\infty$ SBU, (d) trigonal tritopic $M_3OL_3(\text{-Py})_3$ SBU, and (e) cubic octatopic $M_4Cl(L_4)(–\text{tetrazolate})_8$ SBU. Color code: metal, blue; N, green; C, gray; O, red; Cl, pink; terminal ligands, yellow.

potential open metal sites highlighting the corresponding adsorption sites. Two prominent examples where the formation of open metal sites leads to a significant increase in the hydrogen storage capacity are HKUST-1 (Figure 15.5a) and $(Mn_4Cl)_3(L)_4(BTT)_8$ (Figure 15.5e) [10]. In both materials, the open metal sites are formed by thermally assisted evacuation of solvent molecules terminally bound to SBUs. To avoid framework collapse these terminal ligands are typically exchanged for more volatile species (e.g. methanol) prior to evacuation. For further information on the formation of open metal sites, the reader is referred elsewhere [11].

Optimization of the Pore Size With respect to the hydrogen sorption capacity small pores are not necessarily a drawback; in fact, very large pores are intrinsically detrimental to achieving a large hydrogen storage capacity. This is because only those hydrogen molecules that are adsorbed on the inner surface of the pore result in a gain in the adsorption capacity (excess uptake), whereas those near the center of the pore do not interact with the surface of the pore and are simply compressed, similar to the situation in a pressurized gas cylinder (bulk uptake, see Figure 13.1). Considering the size of the hydrogen molecule and the fact that in order to increase the heat of adsorption a more efficient packing leading to stronger interactions must be achieved, it becomes clear that a large free pore volume composed of multiple small pores is more desirable than fewer but larger pores. Large pores in a given framework structure can be divided by interpenetration of frameworks, thus creating a more suitable scenario for hydrogen adsorption, and consequently giving materials with an increased hydrogen sorption capacity. However, it is synthetically challenging to control interpenetration, and as discussed earlier not every framework has an interpenetrated counterpart (see Chapter 2). Reaction parameters such as the concentration of the starting materials, the reaction temperature, or the composition of the solvent mixture can influence whether the interpenetrated or the non-interpenetrated structure will form. We will illustrate the effect of interpenetration on the hydrogen storage capacity using PCN-6 ($Cu(TATB)_2$), a framework of **tbo** topology [12]. A comparison of interpenetrated PCN-6 and non-interpenetrated PCN-6 (called PCN-6′) reveals that PCN-6 adsorbs 1.9 wt% of hydrogen whereas PCN-6′ only adsorbs 0.6 wt% (at 1 bar and 77 K) [13]. A pair of isoreticular expanded analogs of PCN-6 and PCN-6′, termed PCN-9 and PCN-9′, is also known; however, these cannot be activated. A comparison of the structures of PCN-6, PCN-9, and PCN-9′ is given in Figure 15.6. The interpenetrating framework fills the large pore avoiding empty pore volume, thereby increasing the interactions with hydrogen molecules.

While interpenetration can endow MOFs with enhanced mechanical, thermal, and chemical stability, interpenetration of frameworks and the concomitant smaller pores should lead to a lower surface area compared to the non-interpenetrated counterpart. This effect is however often less pronounced than expected. The heat of hydrogen adsorption in interpenetrated structures compared to their non-interpenetrated counterparts is only higher at low loadings.

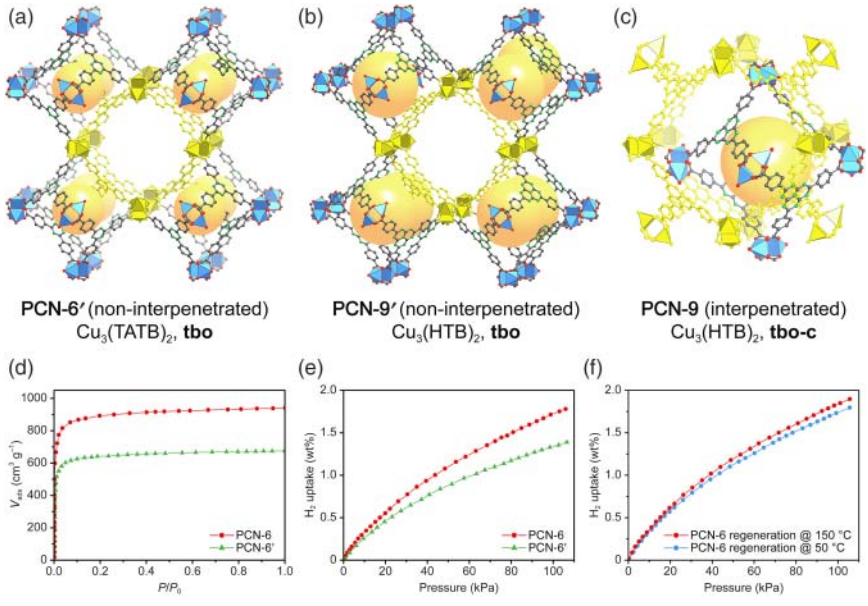

Figure 15.6 (a, b) Comparison of the non-interpenetrated structures of PCN-6′ and PCN-9′ (**tbo**). The small pores are highlighted by orange spheres and the large cubic pores are highlighted as yellow cages. (c) Fragment of the interpenetrated structure of PCN-9. The yellow cage is identical to that shown in the structure of PCN-9′ (b). The interpenetrating framework fills this cage, thereby avoiding large empty pores. Similarly, the structure of PCN-6′ can interpenetrate and the corresponding MOF is termed PCN-6. (d) N_2 adsorption isotherms of PCN-6′ (green triangles) and PCN-6 (red circles) after activation at 50 °C. (e) H_2 adsorption isotherms of PCN-6′ (green triangles) and PCN-6 (red circles) recorded at 77 K after activation at 50 °C. The higher uptake of PCN-6 is ascribed to the smaller pores as a result of framework interpenetration. (f) Comparison of H_2 adsorption isotherms of PCN-6′ activated at 50 °C (blue circles) and 150 °C (red circles) recorded at 77 K. The increased capacity after regeneration at 150 °C is due to the formation of open metal sites. Color code: Cu, blue; C, gray; N, green; O, red.

At intermediate and high loadings, the surface area and the total free pore volume gain importance, respectively. This means that the increase in binding energy due to interpenetration does not outweigh the loss of free pore volume. Consequently, a good material for H_2 sorption should strike a balance between high surface area, a large free pore volume, a high Q_{st} value, and small pore size.

Functionalization The incorporation of functionalized linkers that bear polar or polarizable functional groups has a strong influence on the adsorption behavior of the resulting MOFs. Examples for such a modification are frameworks that contain linkers suitable for metalation by post-synthetic modification (PSM) to create additional strong adsorption sites (Figure 15.7). In some cases, the substitution of one ligand of the metal complexes by hydrogen is facilitated by photolysis as exemplified by $Cr(CO)_3$-functionalized BDC linkers in MOF-5($Cr(CO)_3$) (Figure 15.7c) [11]. Irradiation of this MOF leads to liberation of one CO ligand,

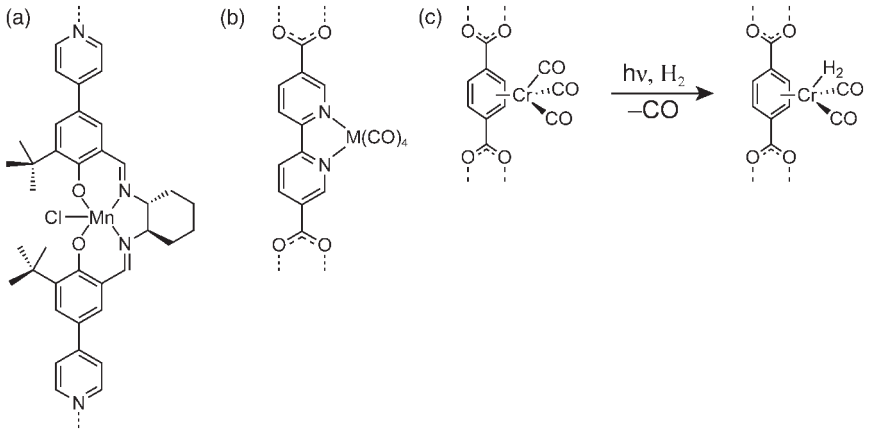

Figure 15.7 (a, b) Introduction of polar adsorption sites by metalation of the organic linker. (c) Functionalization of BDC with $Cr(CO)_3$ and subsequent photochemical decarbonylation creates new binding sites for hydrogen.

and in the presence of hydrogen gas, subsequent H_2 adsorption on the open metal site. The efficiency of this process is however poor and it is not of relevance for applications.

Spillover Hydrogen spillover is the dissociation of H_2 into $H^{\cdot}$ on a metal surface and the consecutive migration and adsorption of these hydrogen atoms onto other materials. This phenomenon is also observed in mixtures of MOFs and precious metal nanoparticles where hydrogen molecules are split into $H^{\cdot}$ atoms on the surface of the metal nanoparticle and subsequently migrate into the pores of the MOF. Spontaneous recombination of $H^{\cdot}$ liberates hydrogen molecules [14]. Drawbacks of such systems are that they typically suffer from low cycling stability and unfavorable desorption kinetics, and in some cases evacuation for more than 12 hours is needed to fully regenerate the material.

15.2.1.3 Use of Lightweight Elements

The formula weight of an adsorbent plays a pivotal role in achieving a high gravimetric uptake. Thus, the use of lightweight elements such as Be^{2+}, Al^{3+}, or Mg^{2+} is highly favorable in designing MOFs with high gravimetric hydrogen uptake. To put this effect into perspective, we consider a comparison of MOF-5 ($Zn_4O(BDC)_3$) and its hypothetical beryllium analog $Be_4O(BDC)_3$. Exchanging the Zn^{2+} ions in MOF-5 by Be^{2+}, the lightest divalent metal, results in an increase in the gravimetric hydrogen storage capacity by 40% [15]. The idea of constructing a compound isostructural to MOF-5 based on $Be_4O(-COO)_6$ SBUs is not too farfetched since molecular analog of this SBU is well-known [16]. The idea of using lightweight elements to construct MOFs with high gravimetric hydrogen capacities is used in the design of $Be_{12}(OH)_{12}(BTB)_4$, the first (and thus far only) beryllium-based MOF. The structure of $Be_{12}(OH)_{12}(BTB)_4$ is built from saddle-shaped 12-c $[Be_{12}(OH)_{12}]^{12+}$ SBUs, a structural element that is unprecedented in molecular beryllium chemistry. These SBUs are joined by

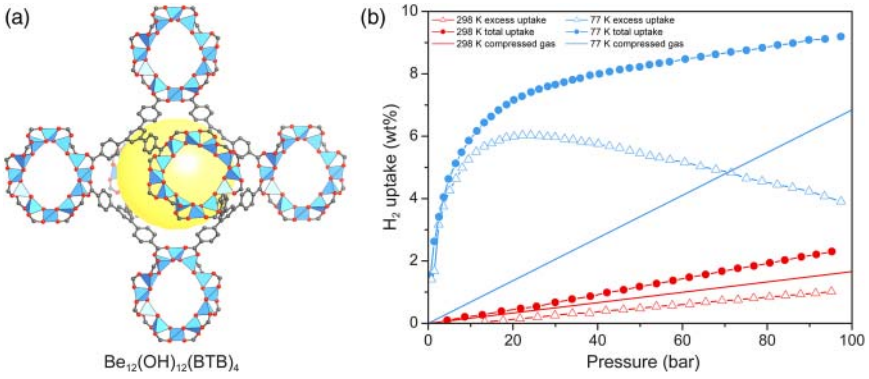

Figure 15.8 (a) Structure of $Be_{12}(OH)_{12}(BTB)_4$. The structure contains a large octahedral pore (yellow ball) surrounded by eight smaller pores (not shown). (b) Hydrogen adsorption isotherms collected at 77 K (blue) and 298 K (red). For both measurements the excess uptake (triangles) and the total uptake (circles) are compared to the density of hydrogen under the respective pressure. Color code: Be, blue; C, gray; O, red.

trigonal BTB linkers to form a framework of **fon** topology [15] (Figure 15.8a). The high gravimetric hydrogen storage capacity of $Be_{12}(OH)_{12}(BTB)_4$ (9.2 wt% at 100 bars and 77 K) is mainly ascribed to its low formula weight since the isosteric heat of hydrogen adsorption is comparatively low ($Q_{st} = -5.5$ kJ mol^{-1}) (Figure 15.8b).

15.2.2 Important MOFs for Hydrogen Storage

The concepts discussed in Section 15.2.1 have been employed in the design and synthesis of many MOFs and their hydrogen storage performance has been studied. Table 15.1 gives a compilation of MOFs and a few selected examples of COFs with interesting hydrogen adsorption properties.

15.3 Methane Storage in MOFs

Unlike hydrogen, methane is a direct fuel, not an energy carrier. It occurs naturally as the main component of natural gas (>95%) and has a high gravimetric heat of combustion (55.7 MJ kg^{-1}), similar to that of gasoline (46.4 MJ kg^{-1}). Among all hydrocarbons methane has the highest RON (107) and is therefore a comparatively clean fuel, which in combination with its compatibility with modern technologies of combustion-based energy production, renders the development of methane storage materials pivotal in transitioning to cleaner fuels. Two current NG storage technologies are its compression at room temperature (200–300 bar) and cryogenic liquefaction. Liquefied natural gas (LNG) has a volumetric energy density (VED) that is only 64% of that of gasoline (22.2 MJ l^{-1} versus 34.2 MJ l^{-1} at −161.5 °C and ambient conditions, respectively), and requires energy-intensive liquefaction, cooling, and storage in expensive cryogenic vessels that suffer from

Table 15.1 Compilation of the surface area and the pore size as well as the gravimetric (wt%) and volumetric (g l^{-1}) hydrogen uptake and the Q_{st} values for zero coverage for a selection of promising hydrogen storage materials.

Chemical formula	Common name	Surface area		Pore size (Å)	Pore volume ($cm^3\ g^{-1}$)	OMS	Hydrogen storage capacity					References
		BET ($m^2\ g^{-1}$)	Langmuir ($m^2\ g^{-1}$)				*p* (bar)	*T* (K)	Uptake (wt%)	Uptake (g l^{-1})	Q_{st} (kJ mol^{-1})	
MOF												
$Be_{12}(OH)_{12}(BTB)_4$		4030	4400			No	1	77	1.6		5.5	[15]
							20 (100)	77	6 (9.2)	(43)		
$Cr_3OF(BDC)_3$	MIL-101		5500	8.6	1.9	Yes	80	77	6.1	1.84	10	[17]
$Cu_3(btc)_2$	HKUST-1		1958			Yes	100	77	3.6		4.5	[18]
$Cu_3(TATB)_2$	PCN-6′		2700		1.045	Yes	1	77	1.35		6	[13]
$Cu_3(TATB)_2$ catenated	PCN-6		3800	5	1.456	Yes	1	77	1.9			[12b]
$Cu_2(tptc)$	NOTT-101	2247		7.3	0.89	Yes	1	77	2.52	43.6	5.5	[19, 20]
$Cu_2(aobtc)$	PCN-10	1047	1779		0.67	Yes	1	77	2.34	18.6	6.8	[21]
$Cu_3(ntei)$	PCN-66	4000	4600		1.63	Yes	1	77	1.79	7.98	6.22	[22]
$Cu_3(ptei)$	PCN-68	5109	6033		2.13	Yes	1	77	1.87	7.2	6.09	[22]
$Cu_3(ttei)$	NU-100	6143			2.82	Yes	1	77	1.82		6.1	[23]
$Cu_3(BHB)$	UTSA-20	1156		3.4, 8.5		Yes	1	77	2.9			[24]
$In_3O(abtc)_{1.5}(NO_3)$	soc-MOF		1417	7.65, 5.95	0.5	Yes	1.2	77	2.61		6.5	[25]
$Mg_2(DOBDC)$	MOF-74	1510				Yes	1	77	2.2		10.3	[26]
$Mn_3[(Mn_4Cl)_3(BTT)_8]_2$	Mn-BTT	2100			0.795	Yes	1.2	77	2.2	43	10.1	[27]

$Mn_3[Mn_4Cl)_3(tpt\text{-}3tz)_8]_2$		1580	1700			No	80	77	3.7 (4.5)	37		[28]
$Ni_3O(TATB)_2$	PCN-5		225		0.13	No	1	77	0.63			[29]
$Zn(mIM)_2$	ZIF-8	1630	1810		0.64	No	1	77	1.27			[30]
							30	77	3.3			
							55	77	3.01			
$Zn_2(abtc)(DMF)_2$	SNU-4		1460		0.53	No	1	77	2.07			[31]
							50	77	3.7			
$Zn_4O(BBC)_2(H_2O)_3\ 3H_2O$	MOF-200	4530	10 400	3.59		No	80	77	7.4 (16.3)	(36)		[3]
$Zn_4O(BDC)_3$	MOF-5	2296	3840			No	50	77	4.7		3.8	[18]
$Zn_4O(BDC)_3$ catenated	MOF-5		1130	6.7		No	1	77	2.0	23.3	7.6	[32]
$Zn_4O(BTB)_2$	MOF-177	4746	5640		1.59	No	70	77	7.5	32		[4]
$Zn_4O(BTB)_{4/3}(NDC)$	MOF-205	4460	6170		2.16	No	80	77	7.0 (12)	(46)		[3]
$Zn_4O(BTE)_{4/3}(BPDC)$	MOF-210	6240	10 400		3.6	No	80	77	8.6 (17.6)	(44)		
$Zn_4O(T_2DC)(BTB)_{4/3}$	UMCM-2	5200	6060			No	46	7	6.9		6.4	[33]
COF												
COF-105		6636 (calc.)		5.22	No	100	77	4.67	18.05			[34]
COF-108		6298 (calc.)		5.59	No	100	77	4.51	17.80			[34]
COF-202			2690		1.09	No	100	298	1.52	8.08		[8a]
COF-202 Li			< 2690		< 1.09	Yes	100	298	4.39	25.86		[8a]

boil-off losses. The compression of natural gas (CNG) requires multistage compressors and heavy thick-walled cylindrical storage tanks. Still VED values of only 27% of that of gasoline are reached (9.2 MJ l^{-1} versus 34.2 MJ l^{-1}). These drawbacks render both LNG and CNG storage impractical for mobile applications. Storing natural gas in tanks filled with solid adsorbents represents a viable alternative. The lower pressures of 35–65 bar needed in such adsorbed natural gas (ANG) tanks and their operation at ambient temperatures eliminate the need for cryogenic or heavy tanks, making it safer and less energy intensive, and consequently also more cost-effective than CNG and LNG storage.

While hydrogen storage in MOFs suffers from intrinsically low isosteric heats of adsorption, the isosteric heats of methane adsorption are typically higher and often in the regime suitable for commercial applications. A high hydrogen storage capacity at ambient temperatures is only realized in the presence of open metal sites in MOFs (or intercalated metal ions in MOFs and COFs) that provide high binding energies (up to 13 kJ mol^{-1}). In contrast, methane typically adsorbs with higher binding energies even to nonpolar organic moieties (e.g. pore openings with multiple adsorptive sites). This adsorption behavior allows for a wider range of suitable materials compared to hydrogen storage. The high surface areas, regular pore shapes, and tunable pore sizes render MOFs superior to traditional porous materials such as zeolites or porous carbons. In the following, we will elucidate how these parameters can be used to design potent methane storage materials.

15.3.1 Optimizing MOFs for Methane Storage

A MOF must fulfill certain prerequisites to be suitable for application in ANG tanks and the most important are (i) the cost to synthesize a given material, (ii) the working capacity, (iii) the cycle stability, and (iv) the chemical stability toward the impurities present in natural gas. While the cost to synthesize a given material is mainly correlated to the demand, the latter three criteria represent intrinsic material properties that can be modified and optimized using the methods discussed in Chapters 1–6.

Methane storage is of particular interest for mobile applications. Here, the working capacity determines the possible driving range with a tank of a given volume. It is defined as the volume of methane stored per volume of material (in $v\,v^{-1}$) in a fully loaded tank (typically at 65 bar) minus the volume that remains in the tank when the depletion pressure (typically 5.8 bar) is reached. This implies that a given material must not only store a large quantity of methane at high pressures but also that a large fraction of this maximum capacity must be available within a pressure window ranging from 5 to 65 bar. Since the magnitude of the working capacity strongly depends on the structure and chemical nature of the MOF, the precise design of its structure and the underlying individual building units is crucial for the development of new high-performance materials. There are several structural factors such as (i) the surface area, (ii) the pore shape, diameter, or aperture, and (iii) the introduction of open metal sites or other strong adsorption sites that can be manipulated and optimized using reticular chemistry.

15.3.1.1 Optimization of the Pore Shape and Metrics

To derive appropriate design principles for MOFs with high methane uptake, it is instructive to first locate the preferred binding sites for methane within the pores of MOFs. Much research has been focused on identifying the primary adsorption sites in MOFs, and similar to other nonpolar gases methane is typically adsorbed close to the SBUs, arguably due to the more polar nature of the SBUs compared to the organic backbone. Additional binding sites are located on the faces and edges of the linker. Even though the interactions arising from these sites are much weaker than those arising from the SBUs, they play a key role in the design of materials with large gas uptake due to their great capacity for an increase in gas loading. Strategies to increase the number of adsorptive sites provided by linker design have been discussed earlier (see Chapter 2) [35]. For methane storage, however, a large surface area does not necessarily correspond to a large working capacity. To illustrate this, we analyze methane adsorption in two **fof** topology frameworks (NOTT-101 and NOTT-103) and a structurally related **stx** topology framework (NOTT-109). These MOFs are similar in terms of their structures but show significant differences in their pore sizes and surface areas (Figure 15.9). NOTT-109

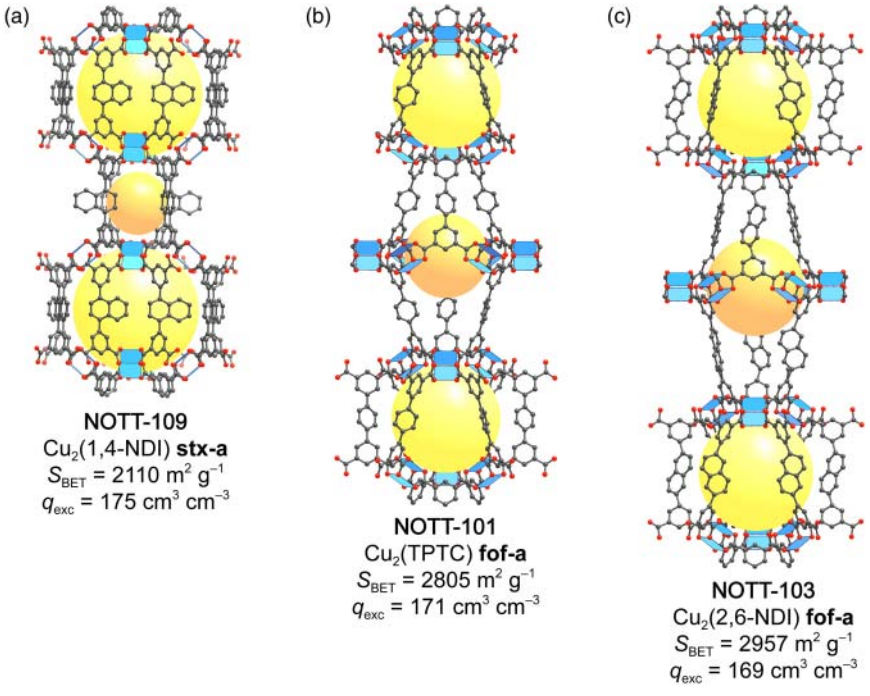

Figure 15.9 (a–c) Crystal structures of NOTT-109, NOTT-101, and NOTT-103 alongside the respective surface areas and excess methane uptake capacities. Although the structures are similar and the surface area increases from (a) to (c) the excess uptake decreases. This highlights the importance of the pore shape and size in realizing a high excess methane uptake. Color code: Cu, blue; C, gray; O, red.

has the lowest surface area ($S_{BET} = 2110\,m^2\,g^{-1}$), followed by NOTT-101 ($S_{BET} = 2805\,m^2\,g^{-1}$) and NOTT-103 ($S_{BET} = 2958\,m^2\,g^{-1}$). The comparison of the excess uptake at room temperature and 35 bar shows that the MOF with the lowest surface area has the highest excess uptake ($q_{exc(NOTT\text{-}109)} = 175\,cm^3\,cm^{-3}$, $q_{exc(NOTT\text{-}103)} = 171\,cm^3\,cm^{-3}$, and $q_{exc(NOTT\text{-}103)} = 169\,cm^3\,cm^{-3}$) [36]. Based on this finding, an empirical formula providing a correlation between the gravimetric methane uptake and the pore volume can be established:

$$q_{exc} = -126.69 \times V_{pore}^2 + 381.62 \times V_{pore} - 12.57 \tag{15.1}$$

where q_{exc} is the excess gravimetric methane storage capacity (at 35 bar and 300 K in $cm^3\,g^{-1}$) and V_{pore} is the free pore volume of the MOF (in $cm^3\,g^{-1}$). Using this empirical equation, the methane storage performance of microporous MOF materials with a pore volume of less than $1.50\,cm^3\,g^{-1}$ can be predicted reasonably well. This example illustrates that not only a large surface area but also appropriately sized and shaped pores are of great importance in realizing a high methane working capacity.

Another important factor to consider when targeting high methane uptake is the optimization of the methane–framework interaction. We illustrate this by comparing the methane uptake characteristics of PCN-61 and PCN-68, two isoreticular frameworks with underlying **rht** topology. PCN-61 is constructed from H_6BTEI linkers and 4-c copper paddle wheel SBUs and its structure features pores of 12, 11.8, and 18.8 Å diameter and a surface area of $3000\,m^2\,g^{-1}$. PCN-68 is the isoreticular expanded analog of PCN-61 and is built from 4-c paddle wheel SBUs and H_6PTEI linkers. Consequently, PCN-68 encompasses larger pores (12, 14.8, and 23.2 Å in diameter) and has a higher surface area ($5109\,m^2\,g^{-1}$) than PCN-61 [22]. Interestingly, PCN-61 still shows a significantly higher volumetric excess methane uptake ($145\,cm^3\,cm^{-3}$) than PCN-68 ($99\,cm^3\,cm^{-3}$), which is attributed to the stronger methane–framework interaction.

A strong interaction between methane and the framework is realized by the introduction of so-called "van der Waal pockets." Such pockets are cages where multiple aryl units are in close proximity, thereby enhancing the dispersive interactions between the adsorbate and the pore surface. Examples of MOFs with structures containing van der Waals pockets are PCN-14 and HKUST-1, two of the best methane storage materials today. PCN-14 is built from 4-c copper paddle wheel SBUs that are connected by ADIP linkers to form a framework of **fof** topology (Figure 15.10) [37]. The structure contains squashed cuboctahedral cages of approximately 12.5 Å diameter and has a comparatively low surface area of only $1753\,m^2\,g^{-1}$. Nevertheless, the high density of anthracenyl units results in enhanced dispersive interactions with the methane molecules and consequently leads to a high gravimetric (15.3 wt%) and volumetric ($220\,cm^3\,cm^{-3}$) uptake.

The importance of appropriately sized pores becomes evident when comparing MOF-210 and Al-**soc**-MOF. The structures of both MOFs have been discussed previously (MOF-210, see Figure 5.9; Al-**soc**-MOF, see Figure 4.14). MOF-210 (**toz**) has two differently sized pores (22×22 Å and 22×51 Å) and a high surface area of $6240\,m^2\,g^{-1}$ [3]. The gravimetric working capacity of $0.376\,g\,g^{-1}$ is one of the highest reported for a MOF. The volumetric capacity of $131\,cm^3\,cm^{-3}$ is

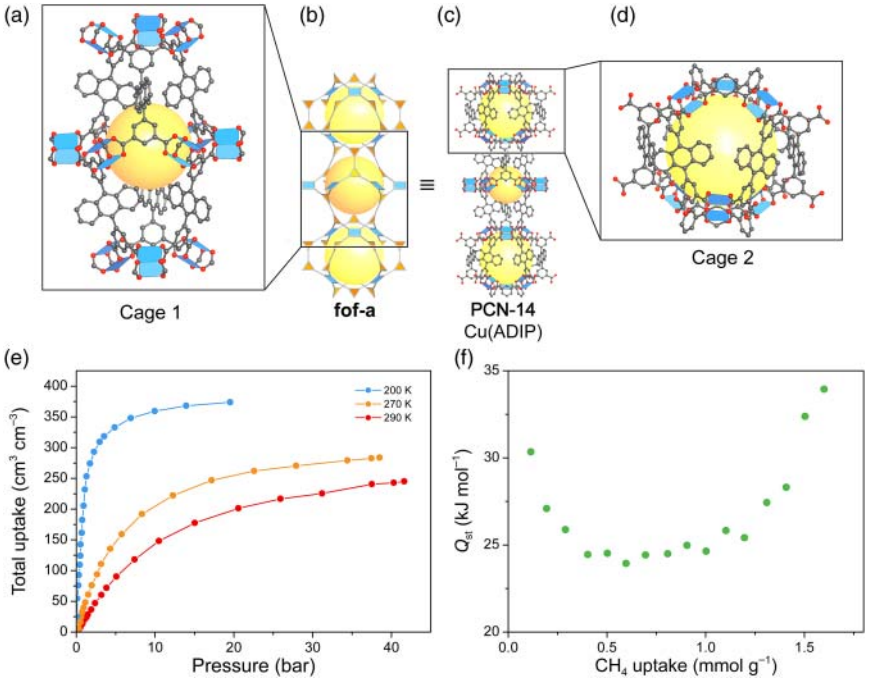

Figure 15.10 (a, d) The two distinct cages in the structure of PCN-14 are shaped in such a way as to maximaze dispersive interactions with methane molecules at the narrow pore apertures. This design feature leads to a high excess methane uptake despite the relatively low surface area of 1753 $m^2\ g^{-1}$. (b) Topology representation (**fof-a**) and (c) crystal structure of PCN-14. (e) Total methane uptake measured at 200 K (blue), 270 K (orange), and 290 K (red). (f) Isosteric heat of methane adsorption calculated for different loadings based on adsorption data collected at 270, 280, and 290 K indicating strong interactions of methane with the framework at low loadings [37]. Color code: Cu, blue; C, gray; O, red.

comparatively low due to the large pore size and pore volume of 3.6 $cm^3\ g^{-1}$.[1] The pores of Al-**soc**-MOF on the other hand are comparatively small (14.3 Å diameter), while a large surface area of 5585 $m^2\ g^{-1}$ is maintained. Therefore, it has a similar gravimetric (q_{grav} = 0.37 $g\,g^{-1}$) but significantly higher volumetric uptake (q_{vol} = 176 $cm^3\ cm^{-3}$) than MOF-210. The examples discussed so far highlight that small pores and narrow passages connecting them increase the strength of dispersion forces between the pore surface and incoming gas molecules and are thus beneficial for realizing high methane adsorption capacities. This can be achieved either by interpenetration or by designing MOFs with complex contorted pore systems. The latter principle is employed in the design of ST-1, ST-2, ST-3, and ST-4, a series of tertiary and quarternary MOFs with complex framework structures [38]. A flow diagram illustrating the synthesis and composition of these MOFs is given in Figure 15.11a. All structures are highly complex and are built from up to five different types of cage (ST-1, **muo**; ST-2, **umt**; ST-3, **ith-d**; ST-4, **ott**). The high methane storage capacity of these

1 The working capacity is measured between 65 and 5.8 bar.

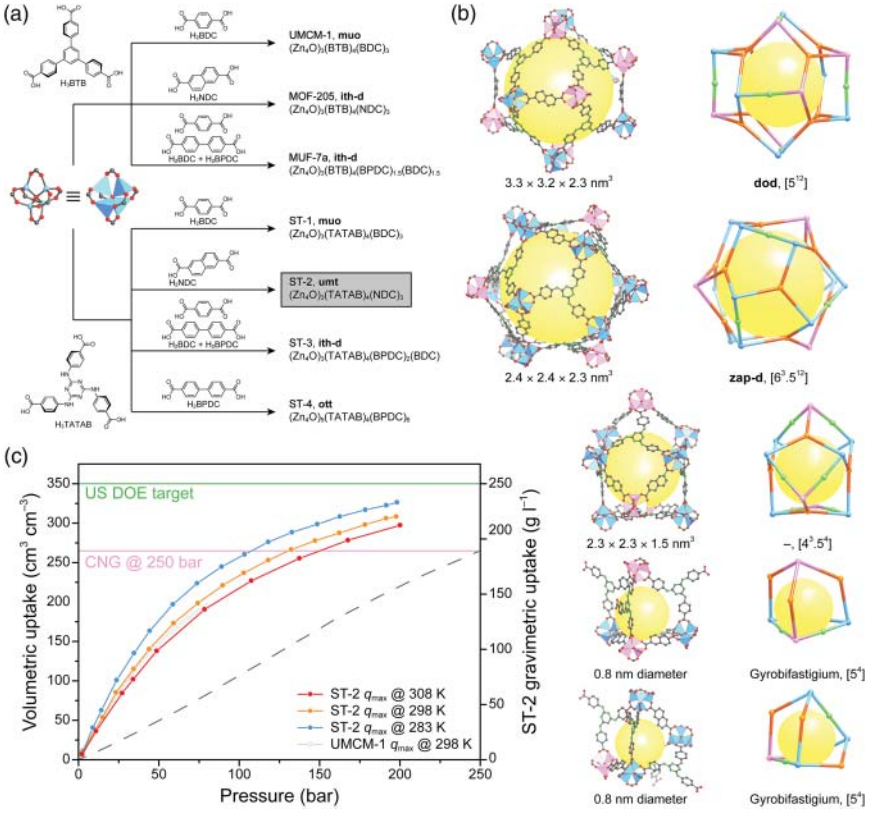

Figure 15.11 (a) Flow diagram visualizing the composition of tertiary and quaternary MOFs constructed from octahedral $Zn_4O(–COO)_6$ SBUs and a combination of linear ditopic and trigonal tritopic linkers. (b) Cages in the **umt** structure of ST-2. The two topologically distinct SBUs are shown in pink and blue. In the topological representation the linear linkers (commonly not show) are represented by green spheres for clarity; however, they do not represent vertices. All cages with exception of the $[5^4]$ cages feature small "van der Waals" pockets and narrow pore openings. Additionally, the walls of the pores are lined with polar TATAB units. (c) Methane adsorption isotherms of ST-2 recorded at 283 K (blue), 298 K (orange), and 308 K (red) alongside a methane adsorption isotherm of UMCM-1 (gray) for comparison [38]. At a pressure of 135 bar ST-2 surpasses the capacity of compressed natural gas at 250 bar (light pink). All hydrogen atoms are omitted for clarity. Color code for crystal structure drawings: Zn, pink and blue; N, green; C, gray; O, red. Color code for the topology representation: 6-c SBUs, pink and blue; trigonal linker, orange; linear linker, green. The yellow spheres indicate the empty space within the respective cage.

compounds originates from the complex interconnected pore systems. Owing to a low methane uptake at pressures below the minimum delivery pressure, all four materials feature a high working capacity. Here, we discuss the best performing member of this series, ST-2. The **umt** net of ST-2 is constructed from four topologically distinguishable cages that are fused to form a highly complex pore system (Figure 15.11b). With the exception of the two topologically identical $[5^4]$ cages, all cages feature polar TATAB units, small "pockets," and – with respect

to the dimensions of the cages – relatively small apertures. These structural features help increase van der Waals interactions. Figure 15.11c shows methane adsorption isotherms of ST-2 measured at different temperatures. ST-2 clearly surpasses the storage capacity of compressed natural gas tanks at pressures >135 bar. The contorted pore system makes it possible to achieve both high volumetric (290 cm^3 cm^{-3}) and gravimetric (206 $g\,l^{-1}$) deliverable capacities between 5 and 200 bar.

15.3.1.2 Introduction of Polar Adsorption Sites

Similar to hydrogen, methane can interact with open metal sites, which leads to increased heats of adsorption. We introduced a selection of SBUs with potential open metal sites earlier in this chapter and the reader is referred to this section for further information. The plot of the total methane uptake against the pore volume of several MOFs shown in Figure 15.12 illustrates that as the pore volume increases, the total volumetric uptake first increases to reach a maximum and then decreases again. This implies that there is an upper limit to the methane storage capacity of framework materials at 65 bar and room temperature at a pore volume of about 1 cm^3 g^{-1}. Only three MOFs, namely HKUST-1, NiMOF-74, and UTSA-76, surpass this maximum. HKUST-1 and NiMOF-74 have some of the highest concentrations of open metal sites in MOFs, and UTSA-76 has a high density of functional pyrimidine groups.

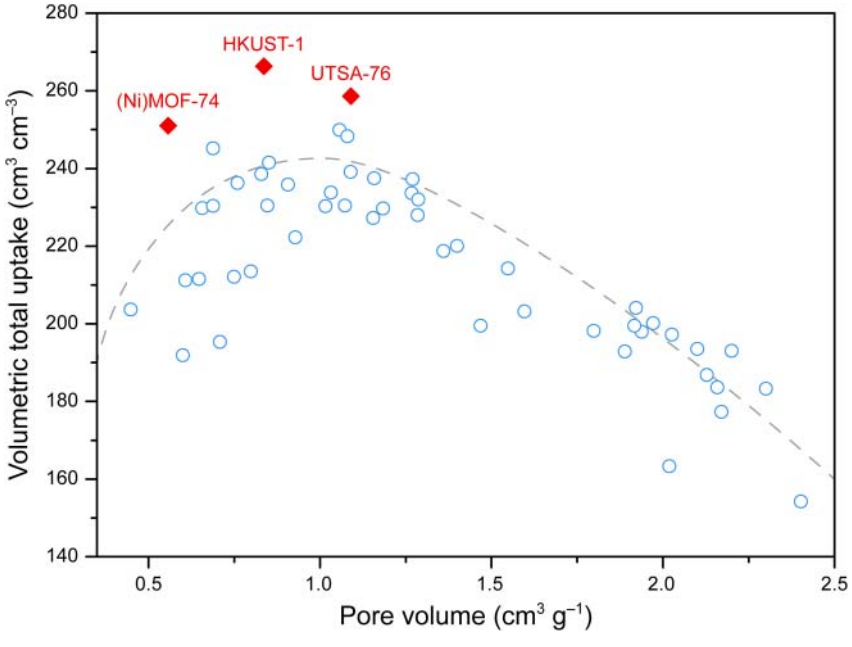

Figure 15.12 Correlation between the volumetric total methane uptake (cm^3 cm^{-3} at 65 bar and 298 K) and the pore volume, V_p (cm^3 g^{-1}). MOFs with open metal sites (HKUST-1 and (Ni)MOF-74) or high concentrations of polar entities dangling into the pores (UTSA-76) show higher volumetric capacities than MOFs without these features (blue circles).

Table 15.2 Compilation of the surface area, the pore size, and the gravimetric (wt%) and volumetric ($cm^3\ cm^{-3}$) methane uptake for a selection of promising MOFs and COFs.

Chemical formula	Common name	Surface area		Pore size (Å)	Pore volume ($cm^3\ g^{-1}$)	OMS	Methane storage capacity				References
		BET ($m^2\ g^{-1}$)	Langmuir ($m^2\ g^{-1}$)				*p* (bar)	*T* (K)	Uptake (wt%)	Uptake ($cm^3\ cm^{-3}$)	
MOF											
$Al_8(OH)_8(BTB)_4(H_2BTB)_4$	MOF-519	2400	2660	7.6 Å	0.938	No	35	298	—	200	[41]
$Al_8(OH)_8(BTB)_4(COO)_4$	MOF-520	3290	3930	16.2 × 9.9	1.277	No	35	298	—	162	[41]
$Al_3O(TCPT)_{1.5}(H_2O)_3]Cl^-$	Al-soc-MOF-1	5585	—	–	2.3	Yes	65	298	—	221	[42]
$Cu_2(ADIP)$	PCN-14	1753	2176	—	—	Yes	35	290	15.36	220	[37]
$Cu_3(BTC)_2$	HKUST-1	1850	—	—	0.780	Yes	35	303	—	267	[43]
$Cu_3(BTTTA)$	NU-125	3120	—	—	1.29	Yes	58	298	—	228	[44]
$Cu_2(TPTC)$	NOTT-101a	2805	—	13 × 24, 14	1.08	Yes	35	298	—	237	[36]
$Cu_2(PyDIA)$	UTSA-76a	2820	—	—	1.09	No	35	298	—	211	[45]
Cu(NDDI)	NOTT-103	2958	—	—	1.157	Yes	35	298	—	194	[36]
$Mg_2(DOBDC)$	MgMOF-74	—	1957	—	0.69	Yes	35	298	—	200	[46]
$Ni_2(DOBDC)$	Ni-MOF-74	—	1593	—	0.56	Yes	35	298	—	230	[46]
$Zn_4O(BDC)(BTAC)_{4/3}$	MOF-905	3490	3770	6.0, 18.0	1.34	No	1.1	298	7.7	—	[47]
$Zn_4O(BDC\text{-}Me_2)(BTAC)_{4/3}$	MOF-905-Me2	3640	3920	5.5, 17.6	1.39	No	1.1	298	11.0	—	[47]
$Zn_4O(BDC)_3$	MOF-5	3480	3860	12.8	1.39	No	80	298	22.6	274	[38, 47]
$Zn_4O(BTB)_3$	MOF-177	4700	5060	10.8	1.83	No	80	298	20.5	344	[38, 47]
$(Zn_4O)_3(TATAB)_4(BDC)_3$	ST-1	4412	—	1.3–3.4	2.39	No	80	298	37.3	—	[38]
$(Zn_4O)_3(TATAB)_4(NDC)_3$	ST-2	5172	—	1.3–3.0	2.44	No	80	298	40.1	—	[38]
$(Zn_4O)_3(TATAB)_4(BPDC)_2(BDC)$	ST-3	5660	—	1.3–3.6	2.67	No	80	298	41.0	—	[38]
COF											
$C_{25}H_{24}B_4O_8$	COF-102	3620	4650	12	1.55	No	35	298	17.72	127	[40, 48]
$C_{25}H_{24}B_4O_8 \times x$Li	COF-102 Li	<3620	<4650	<12	<1.55	Yes	35	298	33	327	[40]
$C_{25}H_{24}B_4O_8Si$	COF-103	3530	4630	12	1.54	No	35	298	16.69	108	[40, 48]
$C_{25}H_{24}B_4O_8Si \times x$Li	COF-103 Li	<3530	<4630	<12	<1.54	Yes	35	298	32.75	315	[40]

In a manner akin to that described for hydrogen storage, the methane storage capacity of MOFs can be enhanced by intercalation of Li^+ ions. This method is particularly interesting for COFs due to their intrinsic low affinity toward methane and an increase of the methane uptake by more than 200% is realized by Li^+ intercalation into 3D COFs (COF-102(Li) and COF-103(Li)) compared to the pristine materials [40].

15.3.2 Important MOFs for Methane Storage

MOFs must meet several prerequisites to be suitable candidates for implementation in methane storage applications (ANG storage): (i) a high working capacity (both gravimetric and volumetric), (ii) high cycle stability, and (iii) low cost of production on an industrial scale. Table 15.2 gives a compilation of MOFs with outstanding performance in methane storage as well as selected examples of COFs.

15.4 Summary

In this chapter, we discussed the design of MOFs for use in energy storage (methane and hydrogen) applications. We uncovered structural features that allow for a high uptake of nonpolar gases and ways to implement these features into extended structures. We saw that strongly polarizing structural fragments as well as van der Waals pockets help increase the uptake of methane and hydrogen and that the pore size of the storage materials must be designed with the size of the targeted adsorptive in mind. The importance of a high uptake between 5 and 65 bar due to practical reasons was highlighted and we gave examples of MOFs that show a good storage performance in this pressure range. We concluded each section with tables summarizing the best performing materials for both applications.

References

1 (a) He, Y., Zhou, W., Qian, G., and Chen, B. (2014). Methane storage in metal-organic frameworks. *Chemical Society Reviews* 43 (16): 5657–5678. (b) Simon, C.M., Kim, J., Gomez-Gualdron, D.A. et al. (2015). The materials genome in action: identifying the performance limits for methane storage. *Energy & Environmental Science* 8 (4): 1190–1199. (c) Gomez-Gualdron, D.A., Gutov, O.V., Krungleviciute, V. et al. (2014). Computational design of metal-organic frameworks based on stable zirconium building units for storage and delivery of methane. *Chemistry of Materials* 26 (19): 5632–5639.

2 Dresselhaus, M., Crabtree, G., Buchanan, M. et al. (2004). Basic Research Needs for the Hydrogen Economy: Report on the Basic Energy Sciences Workshop on Hydrogen Production, Storage, and Use. DOESC (USDOE Office of Science (SC)). Argonne, IL: Argonne National Laboratory (ANL).

3 Furukawa, H., Ko, N., Go, Y.B. et al. (2010). Ultrahigh porosity in metal-organic frameworks. *Science* 329 (5990): 424–428.

4 Wong-Foy, A.G., Matzger, A.J., and Yaghi, O.M. (2006). Exceptional H_2 saturation uptake in microporous metal-organic frameworks. *Journal of the American Chemical Society* 128 (11): 3494–3495.

5 Frost, H. and Snurr, R.Q. (2007). Design requirements for metal-organic frameworks as hydrogen storage materials. *The Journal of Physical Chemistry C* 111 (50): 18794–18803.

6 Bae, Y.-S. and Snurr, R.Q. (2010). Optimal isosteric heat of adsorption for hydrogen storage and delivery using metal-organic frameworks. *Microporous and Mesoporous Materials* 132 (1): 300–303.

7 Kubas, G.J. (2001). *Metal Dihydrogen and s-Bond Complexes: Structure, Theory, and Reactivity*. Springer Science & Business Media.

8 (a) Lan, J., Cao, D., and Wang, W. (2010). Li-doped and nondoped covalent organic borosilicate framework for hydrogen storage. *The Journal of Physical Chemistry C* 114 (7): 3108–3114. (b) Cao, D., Lan, J., Wang, W., and Smit, B. (2009). Lithium-doped 3D covalent organic frameworks: high-capacity hydrogen storage materials. *Angewandte Chemie* 121 (26): 4824–4827. (c) Klontzas, E., Tylianakis, E., and Froudakis, G.E. (2009). Hydrogen storage in lithium-functionalized 3-D covalent-organic framework materials. *The Journal of Physical Chemistry C* 113 (50): 21253–21257.

9 (a) Zou, X., Zhou, G., Duan, W. et al. (2010). A chemical modification strategy for hydrogen storage in covalent organic frameworks. *The Journal of Physical Chemistry C* 114 (31): 13402–13407. (b) Xiang, Z., Hu, Z., Yang, W., and Cao, D. (2012). Lithium doping on metal-organic frameworks for enhancing H_2 storage. *International Journal of Hydrogen Energy* 37 (1): 946–950.

10 (a) Chui, S.S.-Y., Lo, S.M.-F., Charmant, J.P.H. et al. (1999). A chemically functionalizable nanoporous material $[Cu_3(TMA)_2(H_2O)]_n$. *Science* 283 (5405): 1148–1150. (b) Dincă, M., Dailly, A., Liu, Y. et al. (2006). Hydrogen storage in a microporous metal-oganic framework with exposed Mn^{2+} coordination sites. *Journal of the American Chemical Society* 128 (51): 16876–16883.

11 Dincă, M. and Long, J.R. (2008). Hydrogen storage in microporous metal-organic frameworks with exposed metal sites. *Angewandte Chemie International Edition* 47 (36): 6766–6779.

12 (a) Sachdeva, S., Pustovarenko, A., Sudhölter, E.J. et al. (2016). Control of interpenetration of copper-based MOFs on supported surfaces by electrochemical synthesis. *CrystEngComm* 18 (22): 4018–4022. (b) Sun, D., Ma, S., Ke, Y. et al. (2006). An interweaving MOF with high hydrogen uptake. *Journal of the American Chemical Society* 128 (12): 3896–3897.

13 Ma, S., Sun, D., Ambrogio, M. et al. (2007). Framework-catenation isomerism in metal-organic frameworks and its impact on hydrogen uptake. *Journal of the American Chemical Society* 129 (7): 1858–1859.

14 (a) Li, Y., Yang, F.H., and Yang, R.T. (2007). Kinetics and mechanistic model for hydrogen spillover on bridged metal-organic frameworks. *The Journal of Physical Chemistry C* 111 (8): 3405–3411. (b) Li, Y. and Yang, R.T. (2006). Significantly enhanced hydrogen storage in metal-organic frameworks via spillover. *Journal of the American Chemical Society* 128 (3): 726–727. (c) Li, Y. and Yang, R.T. (2006). Hydrogen storage in metal-organic frameworks by bridged hydrogen spillover. *Journal of the American Chemical Society* 128

(25): 8136–8137. (d) Li, Y. and Yang, R.T. (2007). Gas adsorption and storage in metal-organic framework MOF-177. *Langmuir* 23 (26): 12937–12944. (e) Li, Y. and Yang, R.T. (2008). Hydrogen storage in metal-organic and covalent-organic frameworks by spillover. *AIChE Journal* 54 (1): 269–279. (f) Liu, Y.-Y., Zeng, J.-L., Zhang, J. et al. (2007). Improved hydrogen storage in the modified metal-organic frameworks by hydrogen spillover effect. *International Journal of Hydrogen Energy* 32 (16): 4005–4010.

15 Sumida, K., Hill, M.R., Horike, S. et al. (2009). Synthesis and hydrogen storage properties of $Be_{12}(OH)_{12}$(1,3,5-benzenetribenzoate)$_4$. *Journal of the American Chemical Society* 131 (42): 15120–15121.

16 (a) Bragg, W. (1923). Crystal structure of basic beryllium acetate. *Nature* 111: 532–532. (b) Pauling, L. and Sherman, J. (1934). The structure of the carboxyl group II. The crystal structure of basic beryllium acetate. *Proceedings of the National Academy of Sciences* 20: 340–345.

17 Latroche, M., Surblé, S., Serre, C. et al. (2006). Hydrogen storage in the giant-pore metal-organic frameworks MIL-100 and MIL-101. *Angewandte Chemie International Edition* 45 (48): 8227–8231.

18 Panella, B., Hirscher, M., Pütter, H., and Müller, U. (2006). Hydrogen adsorption in metal-organic frameworks: Cu-MOFs and Zn-MOFs compared. *Advanced Functional Materials* 16 (4): 520–524.

19 Lin, X., Telepeni, I., Blake, A.J. et al. (2009). High capacity hydrogen adsorption in Cu(II) tetracarboxylate framework materials: the role of pore size, ligand functionalization, and exposed metal sites. *Journal of the American Chemical Society* 131 (6): 2159–2171.

20 Lin, X., Jia, J., Zhao, X. et al. (2006). High H_2 adsorption by coordination-framework materials. *Angewandte Chemie International Edition* 45 (44): 7358–7364.

21 Wang, X.-S., Ma, S., Rauch, K. et al. (2008). Metal-organic frameworks based on double-bond-coupled di-isophthalate linkers with high hydrogen and methane uptakes. *Chemistry of Materials* 20 (9): 3145–3152.

22 Yuan, D., Zhao, D., Sun, D., and Zhou, H.C. (2010). An isoreticular series of metal-organic frameworks with dendritic hexacarboxylate ligands and exceptionally high gas-uptake capacity. *Angewandte Chemie International Edition* 49 (31): 5357–5361.

23 Farha, O.K., Yazaydın, A.Ö., Eryazici, I. et al. (2010). De novo synthesis of a metal-organic framework material featuring ultrahigh surface area and gas storage capacities. *Nature Chemistry* 2 (11): 944–948.

24 Guo, Z., Wu, H., Srinivas, G. et al. (2011). A metal-organic framework with optimized open metal sites and pore spaces for high methane storage at room temperature. *Angewandte Chemie International Edition* 50 (14): 3178–3181.

25 Liu, Y., Eubank, J.F., Cairns, A.J. et al. (2007). Assembly of metal-organic frameworks (MOFs) based on indium-trimer building blocks: a porous MOF with soc topology and high hydrogen storage. *Angewandte Chemie International Edition* 46 (18): 3278–3283.

26 Sumida, K., Brown, C.M., Herm, Z.R. et al. (2011). Hydrogen storage properties and neutron scattering studies of Mg_2(dobdc) – a metal-organic

framework with open Mg^{2+} adsorption sites. *Chemical Communications* 47 (4): 1157–1159.

27 Dinca, M., Dailly, A., Liu, Y. et al. (2006). Hydrogen storage in a microporous metal-organic framework with exposed Mn^{2+} coordination sites. *Journal of the American Chemical Society* 128 (51): 16876–16883.

28 Dinca, M., Dailly, A., Tsay, C., and Long, J.R. (2008). Expanded sodalite-type metal-organic frameworks: increased stability and H_2 adsorption through ligand-directed catenation. *Inorganic Chemistry* 47 (1): 11–13.

29 Ma, S., Wang, X.-S., Manis, E.S. et al. (2007). Metal-organic framework based on a trinickel secondary building unit exhibiting gas-sorption hysteresis. *Inorganic Chemistry* 46 (9): 3432–3434.

30 Park, K.S., Ni, Z., Côté, A.P. et al. (2006). Exceptional chemical and thermal stability of zeolitic imidazolate frameworks. *Proceedings of the National Academy of Sciences* 103 (27): 10186–10191.

31 Lee, Y.G., Moon, H.R., Cheon, Y.E., and Suh, M.P. (2008). A comparison of the H_2 sorption capacities of isostructural metal-organic frameworks with and without accessible metal sites: $[\{Zn_2(abtc)(dmf)_2\}_3]$ and $[\{Cu_2(abtc)(dmf)_2\}_3]$ versus $[\{Cu_2(abtc)\}_3]$. *Angewandte Chemie* 120 (40): 7855–7859.

32 Kim, H., Das, S., Kim, M.G. et al. (2011). Synthesis of phase-pure interpenetrated MOF-5 and its gas sorption properties. *Inorganic Chemistry* 50 (8): 3691–3696.

33 Koh, K., Wong-Foy, A.G., and Matzger, A.J. (2009). A porous coordination copolymer with over 5000 m_2/g BET surface area. *Journal of the American Chemical Society* 131 (12): 4184–4185.

34 (a) Babarao, R. and Jiang, J. (2008). Exceptionally high CO_2 storage in covalent-organic frameworks: atomistic simulation study. *Energy & Environmental Science* 1 (1): 139–143. (b) El-Kaderi, H.M., Hunt, J.R., Mendoza-Cortés, J.L. et al. (2007). Designed synthesis of 3D covalent organic frameworks. *Science* 316 (5822): 268–272.

35 Chae, H.K., Siberio-Pérez, D.Y., Kim, J. et al. (2004). A route to high surface area, porosity and inclusion of large molecules in crystals. *Nature* 427 (6974): 523–527.

36 He, Y., Zhou, W., Yildirim, T., and Chen, B. (2013). A series of metal-organic frameworks with high methane uptake and an empirical equation for predicting methane storage capacity. *Energy & Environmental Science* 6 (9): 2735–2744.

37 Ma, S., Sun, D., Simmons, J.M. et al. (2008). Metal-organic framework from an anthracene derivative containing nanoscopic cages exhibiting high methane uptake. *Journal of the American Chemical Society* 130 (3): 1012–1016.

38 Liang, C.-C., Shi, Z.-L., He, C.-T. et al. (2017). Engineering of pore geometry for ultrahigh capacity methane storage in mesoporous metal-organic frameworks. *Journal of the American Chemical Society* 139 (38): 13300–13303.

39 Li, B., Wen, H.-M., Zhou, W. et al. (2016). Porous metal-organic frameworks: promising materials for methane storage. *Chem* 1 (4): 557–580.

40 Lan, J., Cao, D., and Wang, W. (2009). High uptakes of methane in Li-doped 3D covalent organic frameworks. *Langmuir* 26 (1): 220–226.

41 Gándara, F., Furukawa, H., Lee, S., and Yaghi, O.M. (2014). High methane storage capacity in aluminum metal-organic frameworks. *Journal of the American Chemical Society* 136 (14): 5271–5274.
42 Alezi, D., Belmabkhout, Y., Suyetin, M. et al. (2015). MOF crystal chemistry paving the way to gas storage needs: aluminum-based soc-MOF for CH_4, O_2, and CO_2 storage. *Journal of the American Chemical Society* 137 (41): 13308–13318.
43 Wiersum, A.D., Chang, J.-S., Serre, C., and Llewellyn, P.L. (2013). An adsorbent performance indicator as a first step evaluation of novel sorbents for gas separations: application to metal-organic frameworks. *Langmuir* 29 (10): 3301–3309.
44 Wilmer, C.E., Farha, O.K., Yildirim, T. et al. (2013). Gram-scale, high-yield synthesis of a robust metal-organic framework for storing methane and other gases. *Energy & Environmental Science* 6 (4): 1158–1163.
45 Li, B., Wen, H.-M., Wang, H. et al. (2014). A porous metal-organic framework with dynamic pyrimidine groups exhibiting record high methane storage working capacity. *Journal of the American Chemical Society* 136 (17): 6207–6210.
46 Mason, J.A., Veenstra, M., and Long, J.R. (2014). Evaluating metal-organic frameworks for natural gas storage. *Chemical Science* 5 (1): 32–51.
47 Jiang, J., Furukawa, H., Zhang, Y.-B., and Yaghi, O.M. (2016). High methane storage working capacity in metal-organic frameworks with acrylate links. *Journal of the American Chemical Society* 138 (32): 10244–10251.
48 Furukawa, H. and Yaghi, O.M. (2009). Storage of hydrogen, methane, and carbon dioxide in highly porous covalent organic frameworks for clean energy applications. *Journal of the American Chemical Society* 131 (25): 8875–8883.